

Composite Dyadic Models for Spatio-Temporal Data

Michael R. Schwob¹, Mevin B. Hooten¹, and Vagheesh Narasimhan^{1,2,3}

¹Department of Statistics and Data Sciences,
The University of Texas at Austin

²Department of Integrative Biology, The University of Texas at Austin
³Department of Population Health, Dell Medical School,
The University of Texas at Austin

November 2, 2023

Abstract

Mechanistic statistical models are commonly used to study the flow of biological processes. For example, in landscape genetics, the aim is to infer mechanisms that govern gene flow in populations. Existing statistical approaches in landscape genetics do not account for temporal dependence in the data and may be computationally prohibitive. We infer mechanisms with a Bayesian hierarchical dyadic model that scales well with large data sets and that accounts for spatial and temporal dependence. We construct a fully-connected network comprising spatio-temporal data for the dyadic model and use normalized composite likelihoods to account for the dependence structure in space and time. Our motivation for developing a dyadic model was to account for physical mechanisms commonly found in physical-statistical models. However, a numerical solver is not required in our approach because we model first-order changes directly. We apply our methods to ancient human DNA data to infer the mechanisms that affected human movement in Bronze Age Europe.

Key words: *advection, Bayesian, diffusion, landscape genomics, potential surface*

1 Introduction

Mechanistic statistical models have appeared in atmospheric sciences (Wikle et al., 2001), ecology (Lu et al., 2020), landscape genetics (Hanks and Hooten, 2013), and spatial epidemiology (Hefley et al., 2017). For example, spatial epidemiologists seek to infer the effect of environments on disease spread. Similarly, the field of landscape genetics is focused on understanding how landscape connectivity affects gene flow in populations of organisms. In these applications, the focus is on the mechanism that governs the spatio-temporal process of interest and, consequently, the structure of the observed data in space and time.

Physical-statistical models are commonly used to study spatio-temporal processes by embedding (partial) differential equations at the process level of a hierarchical statistical framework (Berliner, 2003; Berliner et al., 2023). We present a model that is motivated by advection-diffusion differential equations, but that assumes a phenomenological form commonly used to study the flow of processes. We link differential equations with dyadic models to infer the mechanism that governs the flow of the process of interest. Our approach induces dependence structures common in spatio-temporal statistical models and does not require a numerical solver because we analyze first-order changes directly. We apply the proposed model to study landscape genetics. In particular, we seek to infer the mechanisms that govern dispersal and migration in human populations in Bronze Age Europe, where the process of interest is the movement of genes and individuals.

A common approach to landscape genetics involves the use of circuit theory to infer functional connectivity, where spatial data are treated as a spatially-referenced circuit (Hanks and Hooten, 2013). The circuit can be viewed as a network comprising resistors as nodes and pairwise resistance distances as the effective distances between nodes, where resistance distance is usually defined as a function of characteristics in the parametric space. Statistical circuit theoretic approaches are formally coupled with spatial dynamics and are computationally feasible under standard Markov assumptions. We developed a class of models that share these traits that also allow us to account for temporal proximity to isolate processes of

interest and that scales well for large data sets even when deviating from standard Markov assumptions.

We infer spatio-temporal processes by extending a common form of network analysis, where observations are treated as spatially- and temporally-referenced nodes in a network. An edge connects each of these observations to form a fully-connected network $\mathcal{N} = (\mathcal{V}, \mathcal{E})$, where \mathcal{V} and \mathcal{E} denote the set of nodes and edges, respectively. As spatio-temporal data sets continue to grow in size, the analysis of fully-connected networks may become computationally prohibitive. The field of network analysis has experienced an explosion in scalable methodologies to meet the rapid growth in network sizes (Kolaczyk and Csárdi, 2014). One such methodology is dyadic regression, where pairwise outcomes of interest (i.e., edge weights) are regressed on node-level characteristics. Spatial dyadic regression has been used in many fields, including landscape genomics (Wang, 2013), international relations (Graham, 2020), and infectious disease transmissions (Warren et al., 2023). We extend spatial dyadic regression models by motivating them with an underlying first-order physical process model that motivates the flow of the process in space and time. In particular, we relate dyadic regression with advection-diffusion differential equations to visualize the flow of spatio-temporal processes with potential surfaces.

By constructing a fully-connected network, we form a data set that may contain edges that are not meaningful to study the process of interest. Tobler's first law of geography assumes that processes are decreasingly related as their distance increases (Miller, 2004). Additionally, as the temporal lag between nodes increases, the nodes may be decreasingly related. Common procedures following the construction of a fully-connected network are subnetwork identification or graph reduction, where insignificant edges are eliminated from the network (Nguyen et al., 2019); formal tests for nodal dependence can aid such pursuits (Fosdick and Hoff, 2015). Alternatively, the graphical lasso can be used to estimate sparse precision matrices and identify subgraphs (Friedman et al., 2008). We let the model reduce the influence of less relevant edges on posterior inference by weighting the edge-level data

using heterogeneous composite likelihoods. Composite likelihoods (also called fractional or power likelihoods) assign composite weights to the data model, resulting in weighted posterior inference (Holmes and Walker, 2017; Miller and Dunson, 2019). We show that composite weights may significantly improve posterior inference for the latent mechanism. We also relate the proposed composite weighting scheme to standard regularization techniques.

2 Methods

We denote a fully-connected network $\mathcal{N} = (\mathcal{V}, \mathcal{E})$, where $\mathcal{V} = \{v_1, \dots, v_n\}$ is the set of n nodes and $\mathcal{E} = \{e_{12}, \dots, e_{(n-1)n}\}$ is the set of $N = \binom{n}{2}$ edges. Each node is assumed to be spatially- and temporally-referenced. We let \mathbf{x}_i denote covariates at node i and y_{ij} denote the observed weight of edge e_{ij} , which connects nodes i and j . In dyadic regression, the edge weight y_{ij} is treated as the dyadic outcome between nodes i and j .

2.1 The Motivation for Dyadic Regression

Mechanisms that give rise to the pattern of spatial processes are often visualized as potential surfaces, where the gradient of the surface dictates the direction and velocity of the flow of the process (Hooten et al., 2017). The flow of the process in geographic space is analogous to the movement of a ball on the potential surface (see Figure 1). We construct our Bayesian hierarchical dyadic model with an embedded potential surface that is a function of model parameters and processes.

Potential surfaces are often obtained via advection-diffusion differential equations (Teller, 1937). We consider a stochastic differential equation (SDE) written as a Langevin equation of the form

$$\frac{d\boldsymbol{\mu}(t)}{dt} = \mathbf{g}(\boldsymbol{\mu}(t)) + \frac{\boldsymbol{\epsilon}(t)}{dt}, \quad (1)$$

where $\boldsymbol{\mu}(t)$ is the process of interest, $\mathbf{g}(\boldsymbol{\mu}(t))$ is the advection component of the SDE, and $\boldsymbol{\epsilon}(t)$ is a noise process that is often assumed to be Gaussian. We assume $\{\mu_t\}$ is a discrete

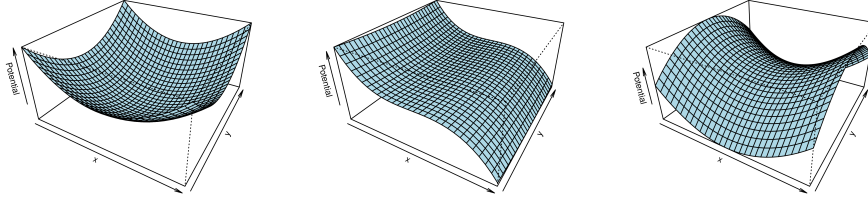


Figure 1: Examples of Potential Surfaces.

one-dimensional process without loss of generality; many spatio-temporal data sets comprise discrete observations of the process of interest. Thus, we consider the Eulerization of (1) $\mu_t - \mu_{t-dt} = g(\mu_{t-dt})dt + \epsilon_t$, which relates the change of the process after a dt time-step with advection and diffusion processes. Brillinger et al. (2012) showed that a potential function $p(\mu_t)$ could be used to model advection such that $g(\mu_t) = -\nabla p(\mu_t)$, where ∇ denotes the gradient operator. Therefore, we write the advection-diffusion differential equation (1) as the Euler discretization

$$\mu_t - \mu_{t-dt} = -\nabla p(\mu_{t-dt})dt + \epsilon_t. \quad (2)$$

The specification in (2) relates the change in the process of interest to the change in the potential function; this intuition forms the foundation for our method to infer spatio-temporal processes.

We relate dyadic regression to the univariate, discretized advection-diffusion differential equation in (2). First, we let t_i denote the temporal reference of node i , and we define $y_{ij} = y_j - y_i$ for all pairs of nodes, where $t_j > t_i$. Conventional dyadic regression models relate the dyadic outcome y_{ij} (i.e., a pairwise difference in the node-level response) to the pairwise difference in node-level covariates. We consider the generalized dyadic model $y_{ij} = -\nabla \pi(\mathbf{x}_i) + \epsilon_{ij}$, which is comparable to (2) where $\pi(\mathbf{x}_i)$ is the function of covariates at node i and ϵ_{ij} is Gaussian noise. We let $-\nabla \pi(\mathbf{x}_i)$ denote a function of the difference in node-level covariates between nodes i and j , which is analogous to the advective component $-\nabla p(\mu_{t-dt})dt$ in (2). Therefore, the mean structure of conventional dyadic models can

represent the gradient of a potential function.

2.2 Composite Likelihoods

Spatio-temporal statistical models assume that observations are decreasingly dependent as spatial and temporal lags increase (Cressie and Wikle, 2015). Thus, dyads associated with nodes that are distant in space or time may inaccurately represent the diffusion of the process, hence obscuring the mechanism. We expect to learn more about the potential surface with dyads comprising correlated nodes than dyads comprising uncorrelated nodes. Therefore, we use composite likelihoods to attenuate the contribution of dyadic outcomes on posterior inference.

Composite likelihoods have become popular in Bayesian statistics, where likelihoods are raised to a composite weight w to allow for Bayesian learning under model misspecification (Holmes and Walker, 2017), to robustify Bayesian inference via coarsening (Miller and Dunson, 2019), or to account for overdispersion in count data (Fletcher et al., 2023). For example, we consider the misspecified model $[\mathbf{y}|\boldsymbol{\alpha}]$ with prior $[\boldsymbol{\alpha}]$, where $[\cdot|\cdot]$ represents the conditional probability density or mass function (Gelfand and Smith, 1990). Then, a coherent and formal Bayesian update of the prior $[\boldsymbol{\alpha}]$ to the posterior $[\boldsymbol{\alpha}|\mathbf{y}]$ exists and is of the form

$$[\boldsymbol{\alpha}|\mathbf{y}]_w \propto [\mathbf{y}|\boldsymbol{\alpha}]^w [\boldsymbol{\alpha}], \quad (3)$$

where w is a composite weight that calibrates the two loss functions $-\log[\boldsymbol{\alpha}]$ and $-\log[\mathbf{y}|\boldsymbol{\alpha}]$ (Holmes and Walker, 2017). Although we use composite weights in a Bayesian context, non-Bayesian methods have been developed that place heterogeneous weights on likelihoods (Majumder et al., 2021).

Conventional composite weights are specified to be homogeneous across observations. However, we specify the composite weights w_{ij} such that the dyadic response y_{ij} is coarsened by a function of differences in node-level covariates, \mathbf{d}_{ij} . We consider the positive

deterministic function

$$w_{ij} = \exp\{-\boldsymbol{\nu}(\mathbf{d}_{ij})'\boldsymbol{\gamma}\}, \quad (4)$$

where $\boldsymbol{\nu}(\mathbf{d}_{ij})$ are q basis functions with basis coefficients $\boldsymbol{\gamma}$. We let $\mathbf{d}_{ij} = (ds_{ij}, dt_{ij})'$ represent the spatial lag ds_{ij} and temporal lag dt_{ij} between nodes i and j because we aim to relate spatial and temporal proximity to the composite weight. Additionally, we only use first-order differences because we attempt to infer a latent spatio-temporal process linked by a first-order differential equation. In general, \mathbf{d}_{ij} can represent an n -order change in any parametric space that affects the dependence among nodes. We consider monotonically increasing basis functions for $\boldsymbol{\nu}(\mathbf{d}_{ij})$ and constrain $\gamma_i > 0$, $i = 1, \dots, q$, because we assume that observations are decreasingly dependent as ds_{ij} and dt_{ij} increase.

We let $[y_{ij}|\boldsymbol{\psi}]$ denote an unweighted dyadic data model with parameters $\boldsymbol{\psi}$. We normalize the weighted data model

$$[y_{ij}|\boldsymbol{\psi}, \boldsymbol{\gamma}] = \frac{[y_{ij}|\boldsymbol{\psi}]^{w_{ij}}}{\int_{\mathcal{Y}} [y_{ij}|\boldsymbol{\psi}]^{w_{ij}} dy_{ij}}, \quad (5)$$

so that it is generative, where \mathcal{Y} is the support for y_{ij} . The weighted data model (5) is analytically tractable when $[y_i|\boldsymbol{\psi}]$ belongs to the exponential family with base measure $h(y_{ij}) \propto 1$. We consider $[y_{ij}|\boldsymbol{\psi}]$ to have the exponential family form

$$[y_{ij}|\boldsymbol{\psi}] = h(y_{ij})g(\boldsymbol{\psi}) \exp(\eta(\boldsymbol{\psi})T(y_{ij})). \quad (6)$$

When powering (6) by the composite weight w_{ij} , we obtain

$$[y_{ij}|\boldsymbol{\psi}]^{w_{ij}} \propto \exp(w_{ij}\eta(\boldsymbol{\psi})T(y_{ij})), \quad (7)$$

where the natural parameters $\eta(\boldsymbol{\psi})$ are scaled by w_{ij} . The powered data model (7) is proportional to the kernel of the unweighted data model $[y_{ij}|\boldsymbol{\psi}]$ with scaled natural parameters $w_{ij}\eta(\boldsymbol{\psi})$. Thus, the normalized weighted data model $[y_{ij}|\boldsymbol{\psi}, \boldsymbol{\gamma}]$ belongs to the same family of distributions as the unweighted data model $[y_{ij}|\boldsymbol{\psi}]$.

Because dyadic regressions typically assume Gaussian noise, we consider a normal data model in the case studies that follow. That is, we let y_{ij} be normally distributed with mean $\tilde{\mathbf{x}}'_{ij}\boldsymbol{\beta}$ and variance σ_y^2 , where $\tilde{\mathbf{x}}_{ij} = \mathbf{x}_j - \mathbf{x}_i$ are the differenced node-level covariates and $\boldsymbol{\beta}$ are regression coefficients. Then, the natural parameters in (7) are $\boldsymbol{\eta}(\psi) = (\tilde{\mathbf{x}}'_{ij}\boldsymbol{\beta}/\sigma_y^2, -1/(2\sigma_y^2))'$ and the component-wise sufficient statistic is $\{y_{ij}, y_{ij}^2\}$. We let

$$w_{ij}\boldsymbol{\eta}(\psi) = (w_{ij}\tilde{\mathbf{x}}'_{ij}\boldsymbol{\beta}/\sigma_y^2, -w_{ij}/(2\sigma_y^2))'$$

denote the natural parameters in the power likelihood, which implies that the expression in (7) is the kernel of a Gaussian distribution with mean $\tilde{\mathbf{x}}'_{ij}\boldsymbol{\beta}$ and variance σ_y^2/w_{ij} . The variance of the normalized weighted data model is the power function $\sigma_y^2 \exp\{\boldsymbol{\nu}(\mathbf{d}_{ij})'\boldsymbol{\gamma}\}$, which results in identifiable σ_y^2 and $\boldsymbol{\gamma}$. Thus, $\boldsymbol{\gamma}$ can be estimated using standard computational methods.

2.3 Composite Weights & Regularization

The variance of the normalized weighted Gaussian data model increases with the spatial and temporal lags, and σ^2 acts as the nugget effect for the dyadic regression. Thus, the composite weighting scheme has the freedom to shrink globally (via σ^2) and act locally (via $\boldsymbol{\gamma}$). The composite weighting scheme resembles regularization techniques, such as the group lasso (Simon et al., 2013) or the horseshoe prior (Carvalho et al., 2009). Standard regularization techniques aim to reduce model complexity to better learn the inherent structure in data. The proposed composite weighting scheme is similar to regularization but imposes heavier tails on the data model.

The composite weights induce a heterogeneous variance on the dyadic regression. Standard approaches to specifying heterogeneous error variances would result in overparameterization (Conn et al., 2018). However, if the composite weights are defined to be a function of auxiliary data (i.e., first-order changes in parametric space), then the model is not overparameterized. Without composite weights, the mechanism may be obscured because the

construction of non-informative edges in the augmented data set will affect posterior inference on the mean structure. The composite weights allow the model to isolate the dyadic outcomes that contribute most to learning the mechanistic dependence by discovering the correct scale of dependence in space and time.

2.4 AR(1) Case Study

We demonstrate the effect of heterogeneous composite weights on posterior inference with an autoregressive time series. We simulated data from the simple AR(1) Gaussian process

$$y_t \sim N(y_{t-1}, \sigma^2), \quad (8)$$

where $y_0 = 0$, $\sigma^2 = 5$ is the variability in the difference $y_t - y_{t-1}$, and $t \in \mathcal{T} \equiv \{1, \dots, 20\}$ following conventional discrete time series notation. We note that (8) is equivalent to the dyadic regression $y_{(t-1)t} \sim N(0, \sigma^2)$, where $y_{(t-1)t} = y_t - y_{t-1}$; thus, a potential surface cannot be inferred due to the homogeneous mean structure. We assumed a lack of knowledge about the AR(1) data generation and aimed to recover σ^2 and the autoregressive dependence, where \mathcal{T} is treated as a one-dimensional discrete space.

We constructed a fully-connected network comprising nodes at locations \mathcal{T} and edge weights defined as the difference in the node-level responses. We assumed zero-mean edges across the fully-connected network and let

$$y_{ij} \sim N(0, \sigma^2), \quad (9)$$

where $i, j \in \mathcal{T}$ and $j > i$. We note that (9) is correctly specified when regressing only on edges where $dt_{ij} = 1$. The normalized weighted data model is

$$[y_{ij} | \sigma^2, w_{ij}] \equiv \frac{[y_{ij} | \sigma^2]^{w_{ij}}}{\int_{\mathcal{Y}} [y_{ij} | \sigma^2]^{w_{ij}} dy_{ij}}, \quad (10)$$

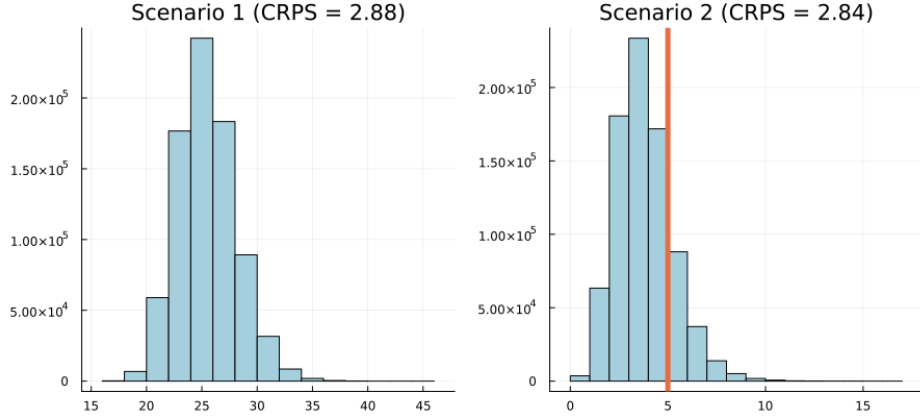


Figure 2: Marginal posterior histograms for σ^2 under scenarios 1 and 2. The red vertical line indicates the true value for σ^2 . Continuous-rank probability scores (CRPS) are included for both scenarios.

where $[y_{ij}|\sigma^2]$ is the unweighted data model in (9).

We considered two scenarios to demonstrate the effect that composite weights had on posterior inference resulting from fully-connected networks. First, we regressed the fully-connected network without composite weights; this was equivalent to defining $w_{ij} = 1$ for each edge in (10). Second, we regressed the fully-connected network with composite weights where $\nu_p(dt_{ij})$ were defined as I-splines based on Gaussian cumulative distribution functions with means $(p + 1)/2$ for $p = 1, \dots, 3$; this specification implies that as dt_{ij} increased, the dependence between nodes i and j decreased. In both scenarios, we considered the conjugate prior $\sigma^2 \sim \text{IG}(0.001, 0.001)$ and sampled σ^2 using a Gibbs update. In the second scenario, we considered a $\text{Gamma}(2, 2)$ prior for each γ_p and proposed values for a Metropolis-Hastings update with an adaptively-tuned random-walk (Roberts and Rosenthal, 2009).

In the first scenario, posterior inference for σ^2 was inflated. The 95% posterior credible interval for σ^2 was $(20.83, 31.19)$, which did not capture the true value (see Figure 2). We attributed the inflated posterior inference for σ^2 to the regression on $\binom{T}{2} - T + 1$ edges that connected nodes that were not partially autocorrelated. We included the first scenario to demonstrate that regressing over a fully-connected network without composite weights may result in poor inference, even in the absence of an advection process.

In the second scenario, the posterior inference for σ^2 was significantly improved despite

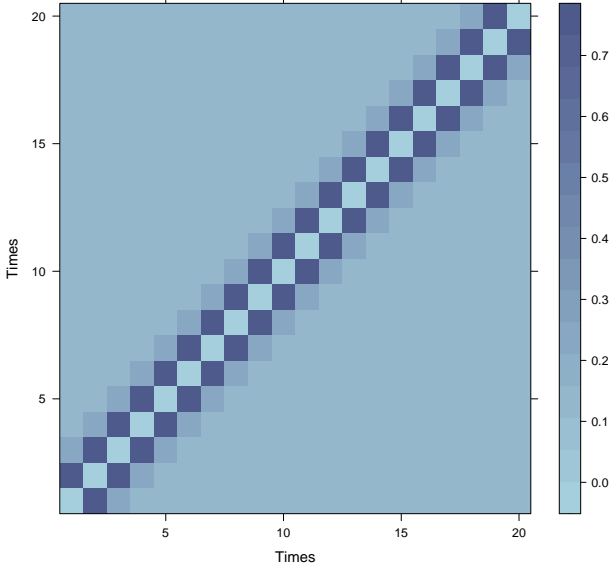


Figure 3: Posterior composite weights per difference in time. The color for each cell represents the inferred composite weight for an edge connecting a node at time t_r and t_c , where t_r and t_c denote the time assigned to the rows and columns, respectively. The values in the diagonal are zero because we do not regress edges with $dt = 0$.

regressing over the same edges as in the first scenario. The 95% posterior credible interval was (1.46, 7.08), which captured the true value for σ^2 . The improvement in posterior inference was evidenced by the lower continuous-rank probability score provided in Figure 2 (Gneiting and Raftery, 2007). Additionally, the inferred composite weights correctly captured the autoregressive process; posterior inference for the composite weights is depicted in Figure 3.

Without knowledge of the temporal process, it may be difficult to determine which edges to construct in a network; this difficulty is exacerbated when inferring spatio-temporal processes. Thus, we constructed a fully-connected network and used composite weights to leverage temporal information that helps us account for mechanistic dependence. The composite weights enabled the model to isolate the dyadic outcomes that contributed the most to learning the mechanistic dependence.

2.5 Dyadic and Spatial Dependence

Dyadic outcomes may exhibit dyadic and spatial dependence. For example, y_{ij} and y_{ik} share a common node and are likely correlated (Lindgren, 2010). Additionally, nodes that are co-located are likely dependent in geographic space. To account for these sources of dependence, we consider the unweighted data model

$$[y_{ij} | \boldsymbol{\beta}, \tilde{\eta}_{ij}, \theta_i, \theta_j, \sigma_y^2] \equiv N(\tilde{\mathbf{x}}'_{ij} \boldsymbol{\beta} + \tilde{\eta}_{ij} + \theta_i + \theta_j, \sigma_y^2), \quad (11)$$

where $\tilde{\eta}_{ij} = \eta(\mathbf{s}_j) - \eta(\mathbf{s}_i)$ are differenced spatial random effects, $\boldsymbol{\eta} = (\eta(\mathbf{s}_1), \dots, \eta(\mathbf{s}_m))'$ are latent spatial random effects at the m distinct node locations $\{\mathbf{s}_i\}$, and $\boldsymbol{\theta} \equiv (\theta_1, \dots, \theta_n)'$ are latent node-level random effects for the n nodes. If each node has a distinct location, then $m = n$. The form of regression model in (11) is conventional when accounting for dyadic and spatial dependence (Warren et al., 2023) and extends multiple matrix regression (Wang, 2013). The random effects $\boldsymbol{\eta}$ and $\boldsymbol{\theta}$ account for latent attributes at the location-level and node-level, respectively, which induces correlation among edges that share a common location or node (Graham, 2020).

Spatial confounding may be present in spatial generalized linear mixed models when both the spatial covariates and latent effects are smooth (Hodges and Reich, 2010; Hughes and Haran, 2013). Thus, we constrain the spatial random effects to be orthogonal to the spatial fixed effects using conditioning by Kriging in an MCMC algorithm (Rue and Held, 2005). We let \mathbf{K} denote the $N \times m$ mapping matrix for $\boldsymbol{\eta}$ in the multivariate version of the unweighted data model (11) and constrain $\boldsymbol{\eta}$ to be orthogonal to $\mathbf{C} = (\mathbf{K}'\mathbf{K})^{-1}\mathbf{K}'\tilde{\mathbf{X}}$, where $\tilde{\mathbf{X}} = (\tilde{\mathbf{x}}_{12}, \dots, \tilde{\mathbf{x}}_{(n-1)n})'$ comprises the pairwise difference in node-level spatial covariates for each dyad. Then, we compute the constrained spatial random effects

$$\boldsymbol{\eta}^* = \boldsymbol{\eta} - \boldsymbol{\Sigma}_\eta \mathbf{C} (\mathbf{C}'\boldsymbol{\Sigma}_\eta \mathbf{C})^{-1} \mathbf{C}'\boldsymbol{\eta},$$

where Σ_η is the full-conditional covariance matrix for $\boldsymbol{\eta}$. Finally, we adjust the posterior variance for $\boldsymbol{\beta}$ to reflect the possible collinearity between the fixed and random effects by sampling

$$\boldsymbol{\beta}^* \sim N(\boldsymbol{\beta}, (\mathbf{C}'\mathbf{C})^{-1}\mathbf{C}'\Sigma_\eta\mathbf{C}(\mathbf{C}'\mathbf{C})^{-1}),$$

where $\boldsymbol{\beta}$ is the original Gibbs update (Hanks et al., 2015).

We specify a spatial Gaussian process for the prior $\boldsymbol{\eta} \sim N(\mathbf{0}, \sigma_\eta^2 \mathbf{R}(\phi))$, where $\mathbf{R}(\phi)_{ij} = \exp(-ds_{ij}/\phi)$ is an exponential-decay covariance function with spatial range ϕ (Cressie, 1991). In our case study, we specify an informative gamma prior for ϕ based on previous landscape genetics analyses. We propose values for ϕ in discrete support Φ , allowing us to compute a finite number of matrices $\mathbf{R}(\phi)$ prior to running the MCMC algorithm and Kriging over the study domain. We used conventional conjugate priors for σ_y^2 , $\boldsymbol{\beta}$, and $\boldsymbol{\theta}$ to facilitate efficient computation. The full Bayesian hierarchical model is provided in Web Appendix A and was implemented in Julia (Bezanson et al., 2017).

2.6 Potential Surface Estimation

The potential surface is of interest when analyzing the flow of a process. In what follows, we assume that each observation of the process of interest varies in its spatial and temporal index. We do not include temporal indices in the node-level covariates \mathbf{x}_i used to compute the potential surface, which inherently is a function of only spatial information. Thus, we denote the covariates at location \mathbf{s}_i as $\mathbf{x}(\mathbf{s}_i)$. The gradient of the potential function in geographic space for the dyadic regression in (11) is

$$-\nabla\pi(\mathbf{x}(\mathbf{s}_i)) = (\mathbf{x}(\mathbf{s}_j) - \mathbf{x}(\mathbf{s}_i))'\boldsymbol{\beta} + (\eta(\mathbf{s}_j) - \eta(\mathbf{s}_i)),$$

which implies the potential function at location \mathbf{s}_i is $\pi(\mathbf{s}_i) = \mathbf{x}(\mathbf{s}_i)'\boldsymbol{\beta} + \eta(\mathbf{s}_i)$. We estimate potential at location \mathbf{s}^* with the posterior mean

$$\text{E}(\pi(\mathbf{s}^*)|\mathbf{y}) = \frac{1}{K} \sum_{k=1}^K \left(\mathbf{x}(\mathbf{s}^*)'\boldsymbol{\beta}^{(k)} + \eta^{(k)}(\mathbf{s}^*) \right),$$

where the (k) superscript denotes the parameter value at the k th MCMC iteration and $\eta^{(k)}(\mathbf{s}^*)$ maximizes

$$[\eta(\mathbf{s}^*)|\boldsymbol{\eta}^{(k)}] = \int \int [\eta(\mathbf{s}^*), \sigma_\eta^{2(k)}, \phi^{(k)}|\boldsymbol{\eta}^{(k)}] d\sigma_\eta^{2(k)} d\phi^{(k)}.$$

We approximate the potential surface by computing $\text{E}(\pi(\mathbf{s}^*)|\mathbf{y})$ for each $\mathbf{s}^* \in \mathcal{S}$, where \mathcal{S} is geostatisticsa fine grid spanning the study domain.

3 Human Migration in Bronze Age Europe

The increasing accessibility of ancient human DNA (aDNA) facilitates our understanding of human history (Mallick et al., 2023). One facet of human history relates to changes in the use of space by ancient populations (Narasimhan et al., 2019). Previous studies have related ancient population genetic structure to the surrounding environment (Novembre et al., 2008). More recently, Frachetti et al. (2017) and Schmid and Schiffels (2023) inferred the mechanism that governed ancient human movement in the highland geography of the Silk Roads and Holocene western Eurasia, respectively. In landscape genetics, such mechanisms are referred to as migratory surfaces (Petkova et al., 2016), which are represented by potential surfaces for gene flow in geographic space.

Migratory surfaces depict the effect that geographic features had on gene flow and are fundamental to understanding how ancient humans interacted with and navigated the environment (Petkova et al., 2016). Our analysis focused on the migratory surface that guided human movement in Bronze Age Europe. We analyzed $n = 398$ sequenced human genomes



Figure 4: Locations of the analyzed sequenced human genomes from Bronze Age Europe.

from the Allen Ancient DNA Resource (Mallick et al., 2023); each genome sequence was dated between 6000-4500 years before the present (BP), recovered in Europe, and sampled in the 1240k library (Rohland et al., 2022). The data comprised the sequenced genome, estimated date of death, and retrieval location.

We treated aDNA samples as spatially- and temporally-indexed nodes in a network. Following standard practice in genomics, we projected the sequenced genomes on a 10-dimensional principal component space for dimension reduction to avoid shrinkage and obtain meaningful constraints for individuals with limited coverage (Patterson et al., 2006). The dyadic outcome y_{ij} was defined as the weighted Euclidean distance in the principal component space between nodes i and j , and weights were computed as the variance explained by each principal component. We used latitude, longitude, time, elevation, and proximity to historic fresh water as the node-level covariates \mathbf{x}_i ; we also considered the squared effects of latitude and longitude, as well as their interaction. Elevation was approximated using a 30 arc second global relief grid (Wessel et al., 2019), and proximity to historic freshwater was computed as the distance between a node location and the centroid of the nearest historic lake (Kelso and Patterson, 2010). Locations of the samples are depicted in Figure 4.

We used the normalized weighted dyadic regression (5) based on the model in (11) to esti-

mate the migratory surface. We regressed genetic dissimilarity y_{ij} on the change in observed environmental covariates $\tilde{\mathbf{x}}_{ij}$ and the change in latent spatial random effects $\tilde{\eta}_{ij}$. We used an informative prior $[\phi] \equiv \text{Gamma}(400, 250)$ for the spatial range in the Gaussian process on $\boldsymbol{\eta}$; these hyperparameters were selected based on exploratory data analyses of ancient human movement during different eras. We specified the set $\Phi = \{0, \dots, \max(\mathbf{ds})/4\}$ with increments of 10 geodesic units, where \mathbf{ds} denotes the vector of pairwise geodesic distances between the observed genetic sequences.

As we demonstrated in the AR(1) case study, composite weights may significantly improve posterior inference when defined as a function of pairwise lags that affect the dependence among nodes. We defined the composite weights as a function of the spatial lag in geodesic meters (ds_{ij}) and temporal lag in years BP (dt_{ij}) between nodes, where we scaled the spatial and temporal lags between edges to be in the unit interval. We specified $\boldsymbol{\nu}(\mathbf{d}_{ij}) = (dt_{ij}, ds_{ij})'$ such that

$$w_{ij} = \exp(-(\gamma_1 dt_{ij} + \gamma_2 ds_{ij})). \quad (12)$$

As the spatial and temporal lags increase, w_{ij} decreases and the heterogeneous variance in the weighted data model increases. Therefore, edges that connect nodes with large spatial and temporal lags have inflated variances and do not obscure the mechanism.

We fit four competing models that only differ in their specification for w_{ij} : (i) Without composite weights (i.e., $w_{ij} = 1$); (ii) with the composite weights in (12) defined only as a function of the temporal lag dt_{ij} (i.e., $\gamma_2 = 0$); (iii) with the composite weights defined only as a function of the spatial lag ds_{ij} (i.e., $\gamma_1 = 0$); and (iv) with the composite weights defined as a function of both dt_{ij} and ds_{ij} . We specified the prior $[\gamma_i] \equiv \text{Gamma}(2, 2)$ for $i = 1, 2$, and we proposed values for a Metropolis-Hastings update using a truncated random-walk on the positive domain. We compared these models using continuous-rank probability scores (CRPS) to demonstrate how accounting for spatial and temporal proximity between nodes affects the model fit.

The first model resulted in the greatest (i.e., worst) CRPS (3.04e-3), likely due to its

inability to account for dependence structures in space or time. Without heteroskedasticity, dyads contributed equally to the estimation of the parameters in the mean structure of the dyadic data model. Thus, edges connecting uncorrelated nodes contributed to the estimation of the potential surface as much as edges connecting correlated nodes.

The second and third models resulted in a CRPS of 2.959e-3 and 3.002e-3, respectively. Therefore, both models fit the observed data better than the model without composite weights. The lower CRPS for the second model implies that accounting for the dependence structure in time improved the model fit more than accounting for the dependence structure in space. Finally, the fourth model resulted in a CRPS of 2.996e-3. The fourth model fit the data better than the first and third model due to the inclusion of temporal lags as an additional auxiliary data source. However, the model with only temporal lags slightly outperformed the model with both temporal and spatial lags.

The proposed method indicates that accounting for temporal dependence in the fully-connected network improves model fit. Spatial dependence likely contributed less to learning the migratory surface because ancient humans could migrate over the entire study domain within one or two generations (Patterson et al., 2012), which is rapid relative to the coarse temporal resolution of the data. Additionally, unlike the temporal domain, movement in spatial domains are bidirectional, which may contribute to the complexity of spatial dependence in the data.

We estimated the potential surface using posterior estimates for β and η from the second model (see Figure 5). The inferred potential surface indicates there are uniformly conducive stretches of land connecting Western Europe to Eurasia that are corridors for gene flow; this supports the hypothesis that pastoralists migrated from the Yamnaya Steppe in Eurasia to Central and Western Europe during this time period (Narasimhan et al., 2019). The posterior potential surface also reveals that northern regions tend to be more resistant to gene flow than southern regions, which further bolsters well-supported theories on ancient human movement throughout Europe (Patterson et al., 2012). The relatively high potential

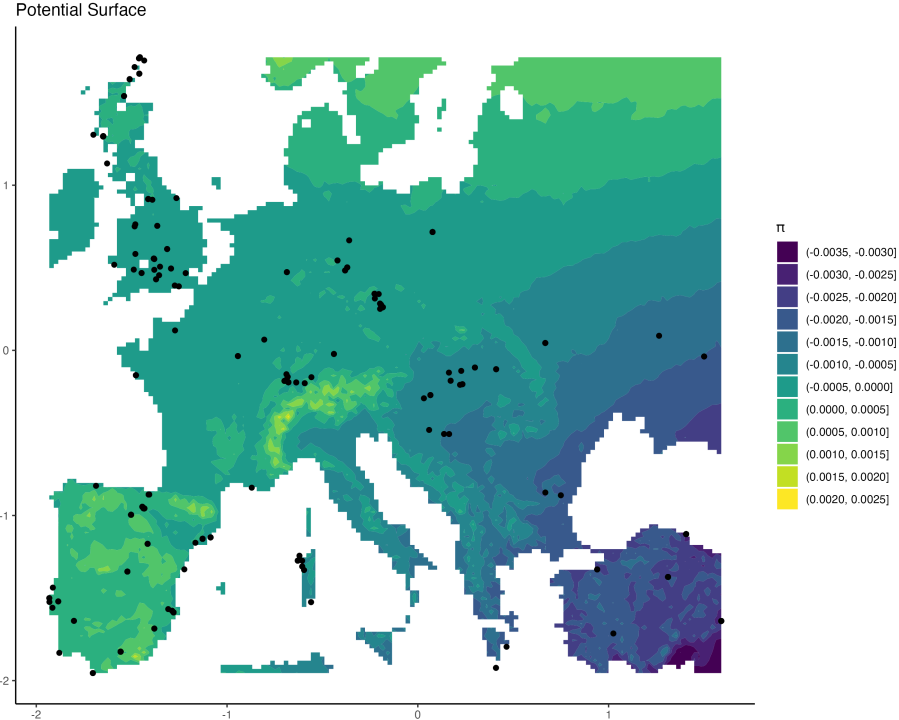


Figure 5: Posterior potential surface for ancient human gene flow in Bronze Age Europe from 6000-4500 BP. Barriers to gene flow are represented by high potential (yellow) regions.

of the Carpathian Mountains, Dinaric Alps, and Swiss Alps compared to the surrounding regions implies that these mountain ranges acted as barriers to gene flow. Finally, coastal regions have lower potential relative to their surrounding areas, which supports the theory that ancient humans often navigated coasts during migration (Bellwood, 2014).

Analysis of the aDNA data set was computationally feasible because our model scales well with larger data sets due to its formulation as dyadic regression; our MCMC algorithm required 171 minutes to obtain 500,000 iterations (49it/s) on a 3.2 GHz processor with 64 GB of RAM. However, the coarseness of the data in space and time presented a challenge. Among the 398 nodes analyzed, the largest pairwise spatial and temporal lags were 508,558 geodesic meters and 1,472 years, respectively. Many edges connected nodes that were distant in space and time. With composite weights, the heterogeneous variances for such edges were larger, and these edges contributed less to the estimation of the potential surface.

4 Discussion

We developed a scalable Bayesian hierarchical framework that allows us to infer spatio-temporal processes using dyadic regression and composite likelihoods. Dyadic regression is used to study the flow of processes across a network, yet most models do not account for the spatio-temporal structure of data despite the dynamics of the process occurring in space and time (Graham, 2020; Warren et al., 2023). We linked these models with advection-diffusion differential equations to infer the mechanism that governs the structure of the data in space and time.

To use dyadic regression, we constructed a network from the spatio-temporal data. Without knowledge of the spatio-temporal process, it is difficult to determine which nodes to connect. Thus, we constructed a fully-connected network and mechanistically modeled the dependence in space and time between nodes using composite likelihoods. The composite weights attenuated the contribution of edges in the fully-connected network using auxiliary information, such as spatial and temporal lags between nodes. Advection-diffusion differential equations relate a temporal change in the process of interest to a change in the space that contains the process. We used composite weights to impose similar dependence in space and time to infer subgraph structures that aid in the estimation of the mechanism.

In spatial statistics, there are several methods to impose dependence structures at the node-level (Cressie, 1991). Common spatio-temporal statistical models such as the (intrinsic) conditional autoregressive model put significant structure on the covariance when assuming that dependence between observations decreases as they grow distant in space and time. In contrast, dyadic regression places such dependence structures on the edges because they do not model node-level data directly (Graham, 2020). We extended dyadic regression to induce dependence structures common in spatio-temporal statistical models.

Computational efficiency was a primary motivation in developing the proposed model. The use of composite weights did not sacrifice conjugacy in the model parameters because composite likelihoods for exponential families with base measures proportional to one be-

long to the same family of distributions as the original unweighted data model. Thus, any conjugacy imposed by the unweighted Gaussian data model will remain after normalizing the weighted data model.

For Gaussian data models, composite weights induce a heterogeneous variance that is a function of spatial and temporal lags. Heteroskedasticity is well-studied in space and time (Wikle and Hooten, 2010; Cressie and Wikle, 2015). If the composite weights are specified as in (4), the unweighted data model variance is the nugget for edges connecting nodes at the same location and time. As spatial and temporal lags increase, the normalized weighted data model variance increases, thereby constraining the model to focus on shorter resolutions in space and time where the process of interest actually occurs. Thus, the composite likelihoods weigh the contribution that each dyad has on posterior inference. A similar concept occurs in weighted least-squares regression, which assigns relatively less weight to ordinates of the empirical semivariogram corresponding to large lags in any parametric space (Cressie, 1985).

We provide a conventional landscape genetics example in Web Appendix B, where we inferred the mechanism that governed gene flow in *Rupicapra rupicapra* populations in the Swiss alps using our dyadic regression model. The resulting inference aligns with that obtained by the circuit theoretic method outlined in Hanks and Hooten (2013); this comparison demonstrates that our method can be used in a variety of settings and provides results similar to conventional landscape genetic methods. However, the *R. rupicapra* case study is limited because the data set does not contain temporal indices. Thus, inference is limited to mechanisms governing the spatial gene flow in *R. rupicapra* populations.

We focused on processes that occur in space and time due to the ubiquity of space-time dynamics in many fields of science. However, our proposed method can infer mechanisms in any parametric space when all nodes have the relevant auxiliary information. For example, potential surfaces outside of geographic space in our aDNA case study could be accommodated, such as mechanisms that affect cultural or demographic processes (Hubisz et al., 2020). It may be challenging to learn potential surfaces in such spaces due to a lack of node-

level auxiliary information. However, in the field of ancient human movement, other data sources, such as archaeological data, can help infer potential surfaces in other parametric spaces, such as technological or cultural practices (Becerra-Valdivia and Higham, 2020).

We constructed a fully-connected network of size $N = \binom{n}{2}$ because we focused on first-order differences between observed nodes. While the proposed dyadic data model is focused on first-order change, our use of composite weights is applicable to any level of change. Applications that are concerned with acceleration through nodes will require analyzing second-order differences between nodes or a difference between edges (Kolaczyk and Csárdi, 2014); such a data set would have size $n(n - 1)(n - 2)/2 > N$. As the order of difference increases, the artificially constructed data set increases in size. Thus, a principled model-based quantity to attenuate the contribution of each differenced outcome may be increasingly helpful in inferring the latent mechanism of interest. Conversely, some studies may be interested in smoothing the observed data set, where collections of nodes are treated as a single unit or hyper-node (Schwob et al., 2019); in such a case, the fabricated data set decreases in size. Although first-order changes are most commonly studied, there is an infinite amount of different orders of change. We demonstrate the use of composite likelihoods for first-order change; however, it may be amenable to all levels of organization.

Acknowledgements

This research was supported by the NSF Graduate Research Fellowship Program.

References

Becerra-Valdivia, L. and Higham, T. (2020). The timing and effect of the earliest human arrivals in North America. *Nature* **584**, 93–97.

Bellwood, P. (2014). *First Migrants: Ancient Migration in Global Perspective*. John Wiley & Sons.

Berliner, L. M. (2003). Physical-statistical modeling in geophysics. *Journal of Geophysical Research: Atmospheres* **108**,

Berliner, L. M., Herbei, R., Wikle, C. K., and Milliff, R. F. (2023). Excursions in the Bayesian treatment of model error. *PloS ONE* **18**, e0286624.

Bezanson, J., Edelman, A., Karpinski, S., and Shah, V. B. (2017). Julia: A fresh approach to numerical computing. *SIAM review* **59**, 65–98.

Brillinger, D. R., Preisler, H. K., Ager, A. A., and Kie, J. (2012). The use of potential functions in modelling animal movement. *Selected Works of David Brillinger* pages 385–409.

Carvalho, C. M., Polson, N. G., and Scott, J. G. (2009). Handling sparsity via the horseshoe. In *Artificial Intelligence and Statistics*, pages 73–80. PMLR.

Conn, P. B., Johnson, D. S., Williams, P. J., Melin, S. R., and Hooten, M. B. (2018). A guide to Bayesian model checking for ecologists. *Ecological Monographs* **88**, 526–542.

Cressie, N. (1985). Fitting variogram models by weighted least squares. *Journal of the International Association for Mathematical Geology* **17**, 563–586.

Cressie, N. (1991). *Statistics for Spatial Data*. John Wiley & Sons.

Cressie, N. and Wikle, C. K. (2015). *Statistics for Spatio-Temporal Data*. John Wiley & Sons.

Fletcher, D., Dillingham, P. W., and Parry, M. (2023). A simple and robust approach to Bayesian modelling of overdispersed data. *Environmental and Ecological Statistics* pages 1–20.

Fosdick, B. K. and Hoff, P. D. (2015). Testing and modeling dependencies between a network and nodal attributes. *Journal of the American Statistical Association* **110**, 1047–1056.

Frachetti, M. D., Smith, C. E., Traub, C. M., and Williams, T. (2017). Nomadic ecology shaped the highland geography of Asia’s Silk Roads. *Nature* **543**, 193–198.

Friedman, J., Hastie, T., and Tibshirani, R. (2008). Sparse inverse covariance estimation with the graphical lasso. *Biostatistics* **9**, 432–441.

Gelfand, A. E. and Smith, A. F. (1990). Sampling-based approaches to calculating marginal densities. *Journal of the American Statistical Association* **85**, 398–409.

Gneiting, T. and Raftery, A. E. (2007). Strictly proper scoring rules, prediction, and estimation. *Journal of the American Statistical Association* **102**, 359–378.

Graham, B. S. (2020). Dyadic regression. *The Econometric Analysis of Network Data* **2020**, 23–40.

Hanks, E. M. and Hooten, M. B. (2013). Circuit theory and model-based inference for landscape connectivity. *Journal of the American Statistical Association* **108**, 22–33.

Hanks, E. M., Schliep, E. M., Hooten, M. B., and Hoeting, J. A. (2015). Restricted spatial regression in practice: Geostatistical models, confounding, and robustness under model misspecification. *Environmetrics* **26**, 243–254.

Hefley, T. J., Hooten, M. B., Hanks, E. M., Russell, R. E., and Walsh, D. P. (2017). Dynamic spatio-temporal models for spatial data. *Spatial Statistics* **20**, 206–220.

Hodges, J. S. and Reich, B. J. (2010). Adding spatially-correlated errors can mess up the fixed effect you love. *The American Statistician* **64**, 325–334.

Holmes, C. C. and Walker, S. G. (2017). Assigning a value to a power likelihood in a general Bayesian model. *Biometrika* **104**, 497–503.

Hooten, M. B., Johnson, D. S., McClintock, B. T., and Morales, J. M. (2017). *Animal Movement: Statistical Models for Telemetry Data*. CRC Press.

Hubisz, M. J., Williams, A. L., and Siepel, A. (2020). Mapping gene flow between ancient hominins through demography-aware inference of the ancestral recombination graph. *PLoS Genetics* **16**, e1008895.

Hughes, J. and Haran, M. (2013). Dimension reduction and alleviation of confounding for spatial generalized linear mixed models. *Journal of the Royal Statistical Society Series B: Statistical Methodology* **75**, 139–159.

Jombart, T. (2008). adegenet: a R package for the multivariate analysis of genetic markers. *Bioinformatics* **24**, 1403–1405.

Kelso, N. V. and Patterson, T. (2010). Introducing natural earth data- naturalearthdata.com. *Geographia Technica* **5**, 25.

Kolaczyk, E. D. and Csárdi, G. (2014). *Statistical Analysis of Network Data with R*, volume 65. Springer.

Lindgren, K.-O. (2010). Dyadic regression in the presence of heteroscedasticity—an assessment of alternative approaches. *Social Networks* **32**, 279–289.

Lu, X., Williams, P. J., Hooten, M. B., Powell, J. A., Womble, J. N., and Bower, M. R. (2020). Nonlinear reaction–diffusion process models improve inference for population dynamics. *Environmetrics* **31**, e2604.

Majumder, S., Biswas, A., Roy, T., Bhandari, S. K., and Basu, A. (2021). Statistical inference based on a new weighted likelihood approach. *Metrika* **84**, 97–120.

Mallick, S., Micco, A., Mah, M., Ringbauer, H., Lazaridis, I., Olalde, I., Patterson, N. J., and Reich, D. E. (2023). The Allen Ancient DNA Resource (AADR): A curated compendium of ancient human genomes. *bioRxiv* pages 2023–04.

Miller, H. J. (2004). Tobler's first law and spatial analysis. *Annals of the Association of American Geographers* **94**, 284–289.

Miller, J. W. and Dunson, D. B. (2019). Robust Bayesian inference via coarsening. *Journal of the American Statistical Association* **114**, 1113–1125.

Narasimhan, V. M., Patterson, N., Moorjani, P., Rohland, N., Bernardo, R., Mallick, S., Lazaridis, I., Nakatsuka, N., Olalde, I., Lipson, M., et al. (2019). The formation of human populations in South and Central Asia. *Science* **365**, eaat7487.

Nguyen, H., Shrestha, S., Tran, D., Shafi, A., Draghici, S., and Nguyen, T. (2019). A comprehensive survey of tools and software for active subnetwork identification. *Frontiers in Genetics* **10**, 155.

Novembre, J., Johnson, T., Bryc, K., Kutalik, Z., Boyko, A. R., Auton, A., Indap, A., King, K. S., Bergmann, S., Nelson, M. R., et al. (2008). Genes mirror geography within Europe. *Nature* **456**, 98–101.

Patterson, N., Moorjani, P., Luo, Y., Mallick, S., Rohland, N., Zhan, Y., Genschoreck, T., Webster, T., and Reich, D. (2012). Ancient admixture in human history. *Genetics* **192**, 1065–1093.

Patterson, N., Price, A. L., and Reich, D. (2006). Population structure and eigenanalysis. *PLoS Genetics* **2**, e190.

Petkova, D., Novembre, J., and Stephens, M. (2016). Visualizing spatial population structure with estimated effective migration surfaces. *Nature Genetics* **48**, 94–100.

Roberts, G. O. and Rosenthal, J. S. (2009). Examples of adaptive MCMC. *Journal of Computational and Graphical Statistics* **18**, 349–367.

Rohland, N., Mallick, S., Mah, M., Maier, R., Patterson, N., and Reich, D. (2022). Three

assays for in-solution enrichment of ancient human DNA at more than a million SNPs. *Genome Research* **32**, 2068–2078.

Rue, H. and Held, L. (2005). *Gaussian Markov Random Fields: Theory and Applications*. CRC Press.

Schmid, C. and Schiffels, S. (2023). Estimating human mobility in Holocene Western Eurasia with large-scale ancient genomic data. *Proceedings of the National Academy of Sciences* **120**, e2218375120.

Schwob, M. R., Zhan, J., and Dempsey, A. (2019). Modeling cell communication with time-dependent signaling hypergraphs. *IEEE/ACM Transactions on Computational Biology and Bioinformatics* **18**, 1151–1163.

Simon, N., Friedman, J., Hastie, T., and Tibshirani, R. (2013). A sparse-group lasso. *Journal of Computational and Graphical Statistics* **22**, 231–245.

Teller, E. (1937). The crossing of potential surfaces. *Journal of Physical Chemistry* **41**, 109–116.

Wang, I. J. (2013). Examining the full effects of landscape heterogeneity on spatial genetic variation: a multiple matrix regression approach for quantifying geographic and ecological isolation. *Evolution* **67**, 3403–3411.

Warren, J., Chitwood, M., Sobkowiak, B., Colijn, C., and Cohen, T. (2023). Spatial modeling of *M. tuberculosis* transmission with dyadic genetic relatedness data. *Biometrics - Early Preview*.

Wessel, P., Luis, J., Uieda, L., Scharroo, R., Wobbe, F., Smith, W. H., and Tian, D. (2019). The Generic Mapping Tools version 6. *Geochemistry, Geophysics, Geosystems* **20**, 5556–5564.

Wikle, C. K. and Hooten, M. B. (2010). A general science-based framework for dynamical spatio-temporal models. *Test* **19**, 417–451.

Wikle, C. K., Milliff, R. F., Nychka, D., and Berliner, L. M. (2001). Spatiotemporal hierarchical Bayesian modeling tropical ocean surface winds. *Journal of the American Statistical Association* **96**, 382–397.

Data Availability

The dataset analyzed during this study is publicly available from the Allen Ancient DNA Resource (Mallick et al., 2023).

Web Appendix A

We fit the following Bayesian hierarchical model in our aDNA case study:

$$[y_{ij}|\boldsymbol{\beta}, \tilde{\eta}_{ij}, \theta_i, \theta_j, \sigma_y^2, \boldsymbol{\gamma}] = \frac{[y_{ij}|\boldsymbol{\beta}, \tilde{\eta}_{ij}, \theta_i, \theta_j, \sigma_y^2]^{w_{ij}}}{\int_{\mathcal{Y}} [y_{ij}|\boldsymbol{\beta}, \tilde{\eta}_{ij}, \theta_i, \theta_j, \sigma_y^2]^{w_{ij}} dy_{ij}},$$

$$\boldsymbol{\beta} \sim N(\mathbf{0}, 10^6 \mathbf{I}),$$

$$\boldsymbol{\eta} \sim N(\mathbf{0}, \sigma_{\eta}^2 \mathbf{R}(\phi)),$$

$$\boldsymbol{\theta} \sim N(\mathbf{0}, \sigma_{\theta}^2 \mathbf{I}),$$

$$\sigma_y^2 \sim IG(0.01, 0.01),$$

$$\sigma_{\eta}^2 \sim IG(0.01, 0.01),$$

$$\sigma_{\theta}^2 \sim IG(0.01, 0.01),$$

$$\phi \sim \text{Gamma}(400, 250),$$

$$w_{ij} = \exp(-(\gamma_1 dt_{ij} + \gamma_2 ds_{ij})),$$

$$\gamma_k \sim \text{Gamma}(2, 2),$$

where $i, j \in \{1, \dots, n\}$, $k \in \{1, 2\}$, and

$$[y_{ij}|\boldsymbol{\beta}, \tilde{\eta}_{ij}, \theta_i, \theta_j, \sigma_y^2] \equiv N(\tilde{\mathbf{x}}_{ij}' \boldsymbol{\beta} + \tilde{\eta}_{ij} + \theta_i + \theta_j, \sigma_y^2).$$

Web Appendix B

We apply the proposed methods to study spatial gene flow in alpine chamois (*Rupicapra rupicapra*) to compare the results of our method with those found in Hanks and Hooten (2013). The alpine chamois is a mountain ungulate native to Europe and is a conserved species in France. The *adegenet* R package described in Jombart (2008) contains microsatellite allele data from nine loci for 335 individual chamois. Each genetic sequence has a spatial reference with elevation data on a 104×80 grid, where each grid cell has an area of 40km^2 . More information on the data can be found in Jombart (2008).

Hanks and Hooten (2013) examined the effect of elevation on gene flow in the alpine chamois population in the Bauges mountains of France. They found a strong nonlinear relationship between elevation and gene flow, with alpine chamois preferring habitats that are moderately high in elevation. Thus, we used elevation and squared elevation as the node-level covariates. For the dyadic outcomes, we computed the Manhattan distance between individuals using the *adegenet* package.

We fit the Bayesian hierarchical model in Web Appendix A with two modifications. First, we used the informative prior $[\phi] \equiv \text{Gamma}(1, 10000)$ for the spatial range parameter based on inference from Jombart (2008). Second, we fixed $\gamma_1 = 0$ because the data set does not contain temporal indices per observation. The resulting posterior $\mathbf{x}'\boldsymbol{\beta}$ surface in Figure 6a aligns with the inference provided in Figure 3c of Hanks and Hooten (2013). However, the posterior latent $\boldsymbol{\eta}$ surface obscures the $\mathbf{x}'\boldsymbol{\beta}$ surface when computing the potential surface (see Figure 6b); this suggests that there are fine-scale processes governing gene flow in the region that were not recovered by the circuit theoretic method. Figure 7 depicts that, on average, regions in the Bauges mountains with elevation slightly greater than 1500m offer the lowest potential (highest conductance) to gene flow in the chamois population; Figure 3b in Hanks and Hooten (2013) supports this finding.

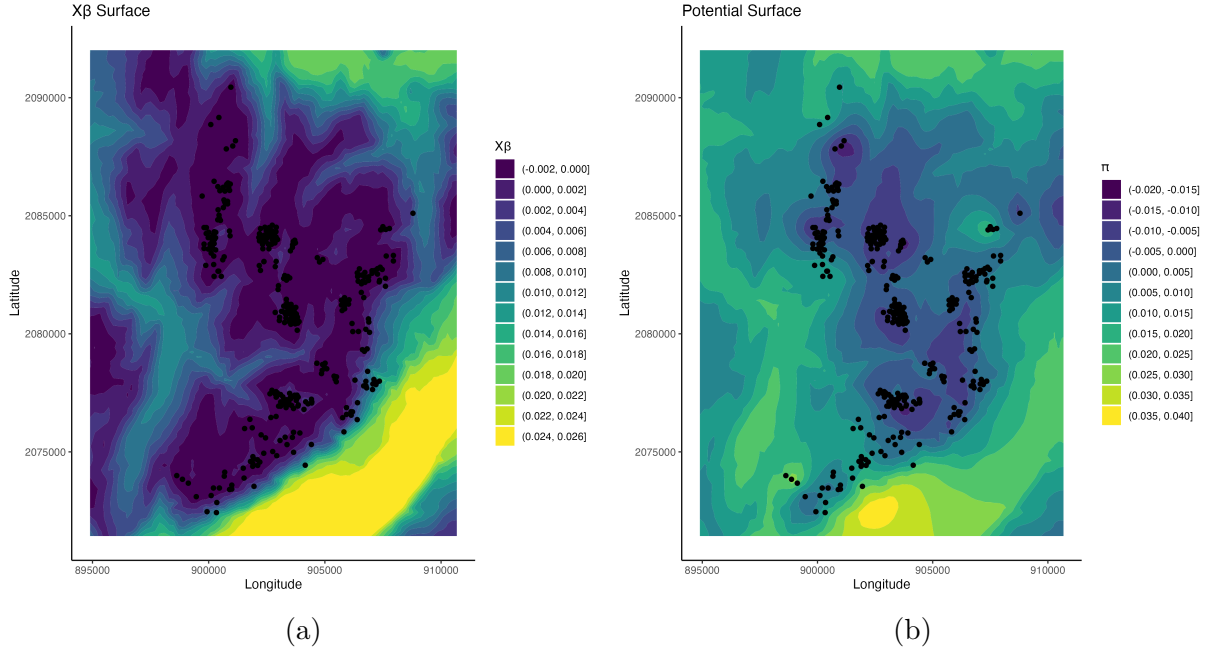


Figure 6: (a) The posterior $\mathbf{x}'\boldsymbol{\beta}$ surface for *R. rupicapra* gene flow in the Bauges mountains of France. Regions with lower values contribute less to the potential surface, indicating they offer more conductance to gene flow. (b) The posterior potential surface. Regions with high potential correspond to regions with high resistance in the circuit theoretic perspective. Similarly, regions with low potential correspond to regions with high conductance for gene flow.

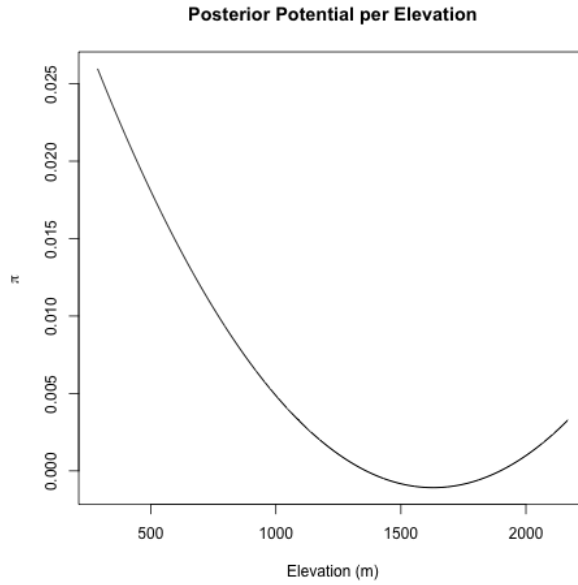


Figure 7: The posterior potential per elevation. Elevations slightly over 1500m have the lowest potential, indicating they provide the highest conductance to gene flow in the chamois population.